Physica B: Condensed Matter 531 (2018) 171–179

Contents lists available at ScienceDirect

Physica B: Condensed Matter

journal homepage: www.elsevier.com/locate/physb

Thermoluminescence due to tunneling in nanodosimetric materials: A Monte Carlo study

Vasilis Pagonis *, Phuc Truong

Physics Department, McDaniel College, Westminster, MD 21157, USA

ARTICLE INFO

Keywords:
Monte Carlo model
Thermoluminescence
Quantum tunneling
Nanocrystal

ABSTRACT

Thermoluminescence (TL) signals from nanodosimetric materials have been studied extensively during the past twenty years, especially in the area of nanomaterials doped with rare earths. One of the primary effects being studied experimentally have been possible correlations between the nanocrystal size and the shape and magnitude of TL signals. While there is an abundance of experimental studies attempting to establish such correlations, the underlying mechanism is not well understood. This paper is a Monte Carlo simulation study of the effect of nanocrystal size on the TL signals, for materials in which quantum tunneling is the dominant recombination mechanism. TL signals are simulated for a random distribution of electrons and positive ions, by varying the following parameters in the model: the radius of the crystal R, tunneling length a, and the relative concentrations of electrons and ions. The simulations demonstrate that as the radius of the nanocrystals becomes larger, the peaks of the TL glow curves shift towards lower temperatures and changes occur in both peak intensity and peak width. For large crystals with a constant density of positive ions, the TL glow curves reach the analytical limit expected for bulk materials. The commonly used assumption of nearest neighbor interactions is examined within the model, and simulated examples are given in which this assumption breaks down. It is demonstrated that the Monte Carlo method presented in this paper can also be used for linearly modulated infrared stimulated luminescence (LM-IRSL) signals, which are of importance in luminescence dosimetry and luminescence dating applications. New experimental data are presented for Durango apatite, a material which is known to exhibit strong anomalous fading due to tunneling; the experimental data is compared with the model. The relevance of the simulated results for luminescence dosimetry is discussed.

1. Introduction

The study of thermoluminescence (TL) signals from nanodosimetric materials is an active research area, due to the many possible practical applications of such materials in luminescence dosimetry and luminescence dating [1,2]) Several luminescent materials consisting of nanoclusters with only a few atoms have attracted attention, and their synthesis and characterization is an increasingly active research area. In particular it has been shown that their physical properties can be different from those of similar conventional microcrystalline phosphors ([2–5]; and references therein). From a theoretical point of view, it is important to understand the underlying luminescence mechanisms in these materials, with a view towards improving luminescence dosimetry and luminescence dating techniques. Two well established luminescence mechanisms in feldspars, apatites, rare earth doped materials and other important luminescent dosimetric materials are quantum mechanical tunneling, and the associated phenomena of "anomalous fading" and "long afterglow" of luminescence signals [1–19].

It has been suggested that traditional energy band models may not be applicable for some of these nanodosimetric materials, because of the existence of strong spatial correlations between traps and recombination centers. Such spatially correlated systems are also likely to be found in polycrystalline and low-dimensional structures, as well as in materials which underwent high energy/high dose irradiations which create groups of large defects. The luminescence properties of such spatially correlated materials can be simulated by using Monte Carlo techniques.

Fig. 1 shows three types of kinetic models which have been studied using Monte-Carlo methods. Fig. 1a shows the energy scheme in the well-known one trap one recombination center model (OTOR), which is commonly used to describe *delocalized* luminescence phenomena in crystalline solids [6–9]. Previous Monte Carlo work using this type of model is summarized in section 2.1. By contrast, Fig. 1b shows a ground

* Corresponding author.
E-mail address: vpagonis@mcdaniel.edu (V. Pagonis).

https://doi.org/10.1016/j.physb.2017.12.042
Received 7 November 2017; Received in revised form 13 December 2017; Accepted 14 December 2017
Available online 16 December 2017
0921-4526/© 2017 Elsevier B.V. All rights reserved.

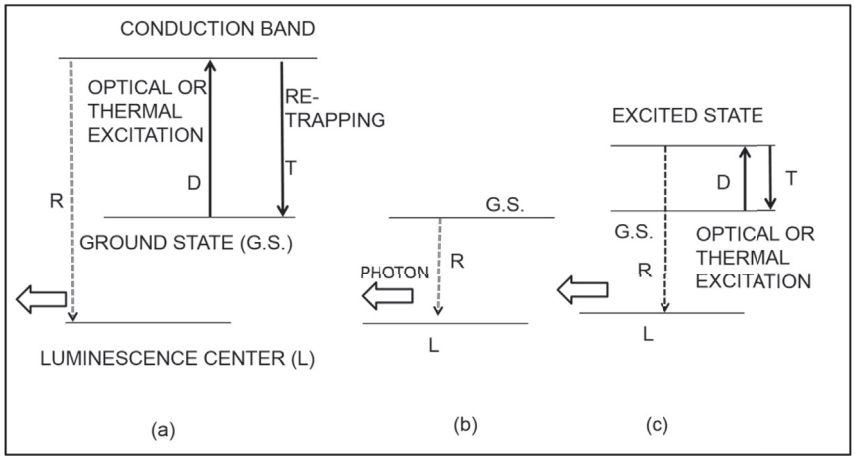

Fig. 1. (a) The energy scheme in the *delocalized* OTOR model, used for describing luminescence phenomena in crystalline solids [6]. (b) The *localized* transition model for tunneling processes taking place from the ground state of the trap [20]. (c) The *localized* transition model for tunneling processes taking place from the excited state of the trap [13], [22]. The various transitions are discussed in the text.

state tunneling model which is based on *localized* energy transitions [10–21]; recent Monte Carlo work using this type of model is summarized in section 2.2. In the third type of model shown in Fig. 1c, electrons can tunnel from the excited state of the electron trap to the luminescence center [13,22,23], and *new* Monte Carlo simulations for this type of model are presented in section 2.3.

In this paper we extend the recent Monte Carlo studies by Pagonis et al. [24], for the case of TL experiments, by performing comparative simulations of crystals of different sizes and charge densities. Specifically this paper examines the effect of crystal size on the TL glow curves from nanocrystals, based on the assumption of a random distribution of electrons and positive ions.

Some advantages of the Monte Carlo techniques are:

- They can be easily extended to include additional physical phenomena in these small crystals.
- They can be used when no analytical equations are available.
- They also provide a microscopic point of view of the luminescence process.

The specific goals of the paper are:

(a) To demonstrate Monte Carlo techniques for simulating a typical TL experiment in a random distribution of electrons and positive ions. These Monte Carlo simulations are based on the extensive previous work for delocalized systems by Mandowski and collaborators [6–9].
(b) To test the Monte Carlo method for *large* crystals, by comparing the simulated TL curves with previously derived analytical equations (Kitis and Pagonis, [14]).
(c) To study crystal size effects on the position and shape of the TL glow peaks, by extending the recent Monte Carlo work by Pagonis et al. [24], for cases in which no analytical expressions are available for the TL glow curves.
(d) To study the effect of various parameters in the model on the TL glow curves, and to discuss the relevance of the simulation results for experimental work.

2. Monte Carlo simulations of luminescence signals in laboratory experiments

This section discusses three different types of luminescence models which can be simulated using Monte Carlo techniques: delocalized models involving the conduction band (section 2.1), localized transitions involving ground state tunneling (section 2.2), and localized transitions involving excited state tunneling (section 2.3). These three models are shown schematically in Fig. 1.

2.1. Previous Monte Carlo simulations based on the delocalized model of Fig. 1a

Fig. 1a shows the energy scheme in the well-known one trap one recombination center model (OTOR), which is commonly used to describe luminescence phenomena in crystalline solids. Several energy transitions are shown schematically: thermal or optical excitation of a carrier from the ground state of the electron trap into the conduction band (solid arrow *D*), retrapping from the conduction band into the trap (solid arrow *T*), and direct recombination transition of electrons from the conduction band into a recombination center (*L*) resulting in the emission of photons (dashed arrow *R*). It is noted that all transitions shown in Fig. 1a represent *delocalized* transition processes, as opposed to the models in Fig. 1b and c which are based on *localized* energy transitions.

Previous TL Monte Carlo work based on Fig. 1a were presented in the papers by Mandowski and collaborators [6–9]. These authors suggested that usually the number of carriers in a sample is very large, and the differential equations used in traditional kinetic models describe the system properly. However, in some solids one must consider clusters of traps as separate systems, since the continuous differential equations are not valid. These authors simulated TL spectra for different trap parameters and different correlations between traps and recombination centers, and compared the resulting TL glow curves with the empirical general order model. For relatively small trap clusters, large differences were found between the modeled TL glow curves and the empirical general order kinetics. These authors showed conclusively that spatially correlated effects become prominent for low concentrations of thermally disconnected traps, and for high recombination situations.

Typically the Monte Carlo calculations are performed with the total population of carriers simultaneously, and in each step of the Monte-Carlo simulation one finds the lowest transition time for all possible transitions, and this is the only transition which is executed. Mandowski et al. [6–9] demonstrated how to perform Monte Carlo calculations in a solid consisting of a number of *separate* systems having the same configuration of energy levels shown in Fig. 1a. Each transition in this scheme is represented mathematically by a transition rate $\lambda(t)$ (s^{-1}) as follows. The rate for thermal excitation (transition *D*) from the trap into the conduction band is $\lambda_{THERMAL}(t) = sexp(-E/kT)$ where *E,s* are the thermal activation energy and frequency factor characterizing the thermal properties of the electron trap. The corresponding optical excitation rate (also transition *D*) is given by $\lambda_{OPTICAL} = \sigma I$ where σ (cm^2) is the optical cross section of the trap and *I* is the photon flux $(photons\ cm^{-2}$

s^{-1}). The retrapping rate for transition T from the conduction band into the trap is given by the product $T = A_n(N\text{-}n)$ where n, N are the number of trapped electrons and total number of traps correspondingly, and A_n is the constant retrapping coefficient for a single carrier into a single trap. The recombination rate (transition R) from the conduction band into the luminescence center (L) is given by the product $R = A_m m$, where m is the number of trapped holes in recombination centers, and A_m is the constant recombination coefficient for a single carrier into a single center.

In each step of the Monte Carlo simulation, the times t_i of each allowed transition are generated for all carriers in the system, and can be evaluated from the integral Eqt (Mandowski and Świątek, [6] 1992, their Eqt (5)):

$$\int_0^{t_i} \lambda(t')dt' = -\ln(a_i), \tag{1}$$

where a_i is a homogeneous normalized random variable from the interval (0, 1) and $\lambda(t)$ (in s^{-1}) is the appropriate transition rate (T, R, or D) for the transition under consideration, as described above. Eqt (1) has simple analytical solutions for the transitions R, T in Fig. 1a, since these transitions do not depend on time. However, in the case of TL experiments Eqt (1) must be solved numerically, as described in section 2.3.

2.2. Previous Monte Carlo simulations based on the localized model of Fig. 1b

In the ground state tunneling model shown in Fig. 1b, electrons can tunnel directly from the ground state of the electron trap into the luminescence center (L). In this model which was considered for example analytically by Tachiya and Mozumder [20], the transition rate $\lambda(t)$ (s^{-1}) for the recombination process is independent of time t, and depends instead on the distance r between the electron and positive ion:

$$\lambda(r) = \frac{1}{\tau(r)} = s' \exp[-r/a], \tag{2}$$

where a is the attenuation length of the wavefunction, s' is the frequency characterizing the ground state tunneling process, and $\tau(r)$ represents the characteristic lifetime.

There are several recent Monte Carlo simulations in the literature, which are based on Eqt (2), and on random distributions of electrons and positive ions. Larsen et al. [10] presented a Monte Carlo model for ground state tunneling which simulated the processes of charge loss and charge creation in feldspar, by assuming that the number density of electrons and holes are equal at all times. Pagonis and Kulp [17] presented a modified quantitative version of the model by Larsen et al. [10], in which the number density of positive ions far exceeds that of electrons. These authors were able to produce quantitative agreement of the Monte Carlo model with experimental data, by simulating the processes of charge loss and charge creation by irradiation in nature. In recent relevant work, Pagonis et al. [21] developed analytical equations for the loss of charge due to tunneling, for arbitrary relative concentrations of electrons and positive ions in a solid. These analytical solutions compared well with the results of Monte Carlo simulations. Also recently Pagonis et al. [24] presented Monte Carlo simulations of the effect of crystal size on ground state tunneling phenomena in nanocrystals. These authors found that the luminescence signals in such systems depend on three characteristic lengths: the radius of the crystal R, the tunneling length a, and the initial average distance $d>$ between electrons and positive ions (which is directly related to the density of charges in the material).

2.3. Monte Carlo simulations of TL based on the localized model of Fig. 1c

During a typical laboratory experiment, one uses optical or thermal excitation, and the dominant process is the recombination process taking place from the excited state of the trapped electron to the recombination center. The relevant *localized* transitions are shown as D,T,R in Fig. 1c; although these transitions have some mathematical similarity to the transitions of the delocalized model of Fig. 1a, the important difference is that they involve the excited state of the trap, instead of taking place via the conduction band.

In a typical TL experiment, the sample is heated with a linear heating rate β (K/s) from a starting temperature T_o up to a high temperature around 500 °C, so that the temperature varies with time t as $T(t) = T_o + \beta t$. Jain et al. [25] and previously Thioulouse et al. [22] and Chang and Thioulouse [23], demonstrated that for this type of experiment Eqt (2) must be replaced by the following Arrhenius type of expression (Jain et al. [25], their Eqts. (3) and (6)):

$$\begin{aligned}\lambda(r,t) = \frac{1}{\tau(r,t)} &= s \exp[-r/a]\exp[-E/(k_B T)] \\ &= s \exp[-r/a]\exp[-E/\{k_B(T_o + \beta t)\}].\end{aligned} \tag{3}$$

where E is the thermal activation energy between the ground state and the excited state of the trapped electron, k_B is the Boltzmann constant and s is the frequency factor characterizing tunneling taking place from the excited state of the system. It is noted that Eqt (3) is derived by assuming quasi-static equilibrium conditions (QE) in the excited state tunneling model of Fig. 1c [22,23,25].

By combining Eqts (1) and (3) we obtain:

$$s \exp[-r/a]\int_0^{t_i} \exp[-E/\{k_B(T_o + \beta t')\}]dt' = -\ln(a_i). \tag{4}$$

The integral in Eqt (4) cannot be replaced by a simple analytical expression. However, one can approximate it to a very good degree of accuracy by using the two terms of the series approximation of the exponential integral function $E_i(T)$ (Chen and Pagonis [26], Chapter 15):

$$\int_0^t \exp[-E/\{k_B(T_o + \beta t')\}]dt' = \frac{k_B T^2}{\beta E}\exp[-E/(k_B T)]\left(1 - \frac{2k_B T}{E}\right) \tag{5}$$

By combining Eqts (4) and (5) we obtain:

$$\left.\begin{aligned} &s \exp[-r/a]\frac{k_B T^2}{\beta E}\exp[-E/(k_B T)]\left(1 - \frac{2k_B T}{E}\right) = -\ln(a_i) \\ &T = T_o + \beta t_i \end{aligned}\right. \tag{6}$$

Eqt (6) is the main equation used to evaluate the times t_i for recombination events during the TL process. Its solution must be obtained numerically in each step of the Monte Carlo simulation and for each remaining electron in the system, as is discussed next.

In the Monte Carlo simulations presented in this paper we follow the same method as Pagonis et al. [24] and Pagonis and Kulp [17], by considering a spherical volume of radius R, and with corresponding initial concentrations of electrons and positive ions n_o, m_o. During the simulation each of the remaining electrons $n(t)$ in the spherical volume is examined, and the nearest neighbor distances r_{MIN} are calculated. The recombination times t_i are calculated for each electron in the system by solving numerically Eqt (6) in the form:

$$\left.\begin{aligned} &s \exp[-r_{MIN}/a]\frac{k_B T^2}{\beta E}\exp[-E/(k_B T)]\left(1 - \frac{2k_B T}{E}\right) = -\ln(a_i) \\ &T = T_o + \beta t_i \end{aligned}\right. \tag{7}$$

Only the event corresponding to the shortest of all the possible times t_i in Eqt (7) happens, i.e. the electron-ion pair corresponding to this shortest time is allowed to recombine. Close-by pairs are more likely to recombine first, and further away pairs are likely to recombine later. After this pair is removed from the system in the simulation, the distances between each electron and the positive ions are re-evaluated, and the minimum t_i time is used to update the total time elapsed from the beginning of the simulation. This process is repeated until there are no more electrons left in the system. The program keeps track of the remaining number of electrons $n(t)$ in the system, and calculates the electron survival probability $P(t) = n(t)/n_o$. The program also keeps track

of the rate of change of the number of electrons $I(t) = -\Delta n/\Delta t$, which is proportional to the experimentally observed TL intensity.

3. Results from the Monte Carlo simulations

In section 3.1 the Monte Carlo algorithm described in section 2.3 is tested for l*arge crystals* with a constant positive ion density ρ, by comparing with analytical expressions available in the literature. Section 3.2 examines the effect of crystal size on the TL glow curves, obtained by varying the relative concentrations of electrons and positive ions. In section 3.3 results are presented for situations where the concentrations of electrons and positive ions are equal at all times. In section 3.4 the commonly made assumption of nearest neighbor interactions is examined, for different charge densities in the system. In section 3.5 it is demonstrated how the simulations in this paper can be extended for the case of linearly modulated infrared stimulated luminescence experiments (LM-IRSL), which are of interest in feldspars, apatites and other similar materials.

3.1. Large crystals with electron concentration much smaller than the positive ion concentration: comparison with analytical expression

Kitis and Pagonis [14] derived an analytical expression for the electron survival probability during a TL experiment, by using the model of Jain et al. [13]. When the initial concentration of electrons (n_o) is much smaller than the initial concentration of positive ions (m_o), the random distribution of charges can be characterized by an almost constant density of positive ions ρ given by:

$$\rho = \frac{m_o}{4\pi R^3/3}. \tag{8}$$

Kitis and Pagonis [14] showed that in such cases ($n_o \ll m_o$ and nearest neighbor interactions), the survival probability of the electrons is given by the analytical expression:

$$P(t) = n(t)/n_o = \exp\left[-\left(4\pi\rho a^3/3\right)\left[\ln\left\{1 + 1.8\int_0^t s\exp\left[-\frac{E}{k_B(T_o+\beta t')}\right]dt'\right\}\right]^3\right], \tag{9}$$

where a is the tunneling length, $n(t)$ is the remaining number of electrons at time t, and ρ (m^{-3}) represents the actual number density of positive ions per unit volume. By combining Eqts (5) and (9), the following analytical expression is obtained:

$$P(t) = \exp\left[-\left\{4\pi\rho a^3/3\right\}\left[\ln\left\{1 + 1.8\frac{sk_B(T_o+\beta t)^2}{\beta E}e^{-E/\{k_B(T_o+\beta t)\}}\left(1 - \frac{2k_B(T_o+\beta t)}{E}\right)\right\}\right]^3\right] \tag{10}$$

It must be emphasized that this equation is valid for *large* crystals, and that it was derived from a *macroscopic* point of view, by starting with the system of differential Eqts in the model by Jain et al. [13]. The derivative $-dP/dt$ of Eqt (10) is proportional to the TL intensity.

In a preliminary test of the Monte Carlo algorithm, we study the Monte Carlo behavior of a large crystal, and compare it with the analytical Eqt (10). Fig. 2 shows a Monte Carlo simulation of a TL experiment in a spherical distribution of radius $R = 71$ nm, tunneling length $a = 0.71$ nm, constant density of positive ions $\rho = 3x10^{24}$ m^{-3}, activation energy $E = 0.8$ eV, tunneling frequency $s = 3x10^{12}$ s^{-1}. The survival probability $P(t)$ shown in Fig. 2a is the average of 7000 Monte Carlo runs, with each run consisting of an initial number of $n_o = 10$ electrons and $m_o = 1100$ positive ions inside the sphere, i.e. the concentration of electrons is 110 times smaller than the concentration of positive ions. Fig. 2b shows the corresponding simulated TL signal $L(t) = -\Delta n/\Delta t$, calculated from Fig. 2a. In this example, the *dashed* lines in Fig.2ab show the survival probability $P(t)$ from analytical Eqt (10), and its derivative $TL = -dn/dt$ correspondingly; good agreement is seen between the Monte Carlo simulation and the analytical equation. The *solid* lines in Fig. 2ab indicate the numerical solution of the original differential equations in the model by Jain et al. [13].

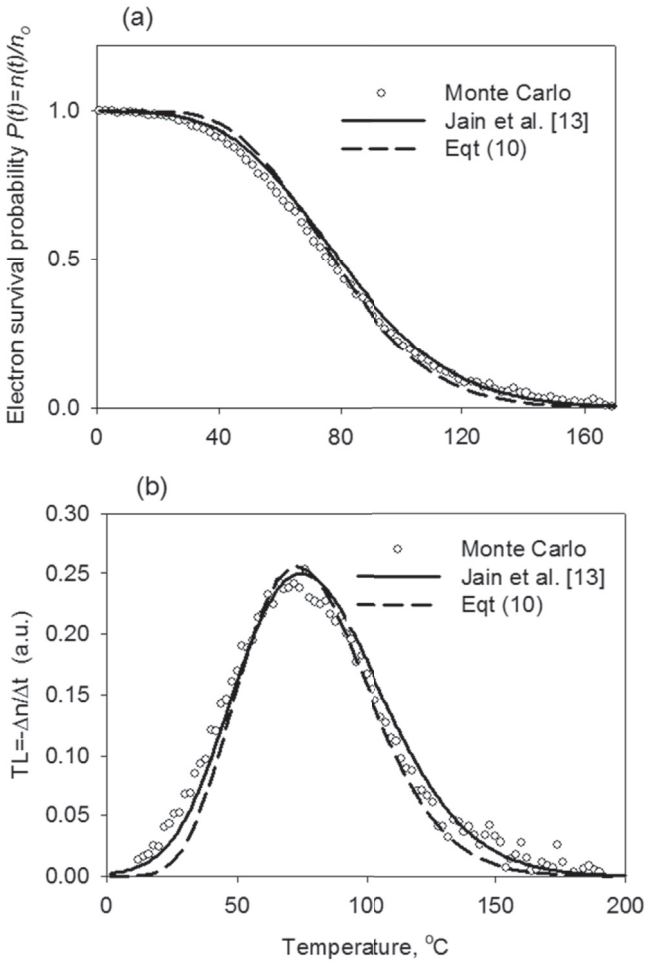

Fig. 2. Monte Carlo simulation of a TL experiment. (a) The survival probability $P(t)$ is the average of 7000 Monte Carlo runs, with each run considering of an initial number of $n_o = 10$ electrons and $m_o = 1100$ positive ions inside the sphere. The *dashed* lines are the survival probability $P(t)$ from analytical Eqt (10), and the *solid* lines indicate the numerical solution of the original differential equations in the model by Jain et al. [13]. (b) The corresponding simulated TL signal $L(t) = -\Delta n/\Delta t$, calculated from (a).

3.2. The effect of relative concentrations of electrons and positive ions on the TL glow curves

Fig. 3 shows a Monte Carlo simulation of a TL experiment in the same spherical distribution as in Fig. 2, by varying the relative initial

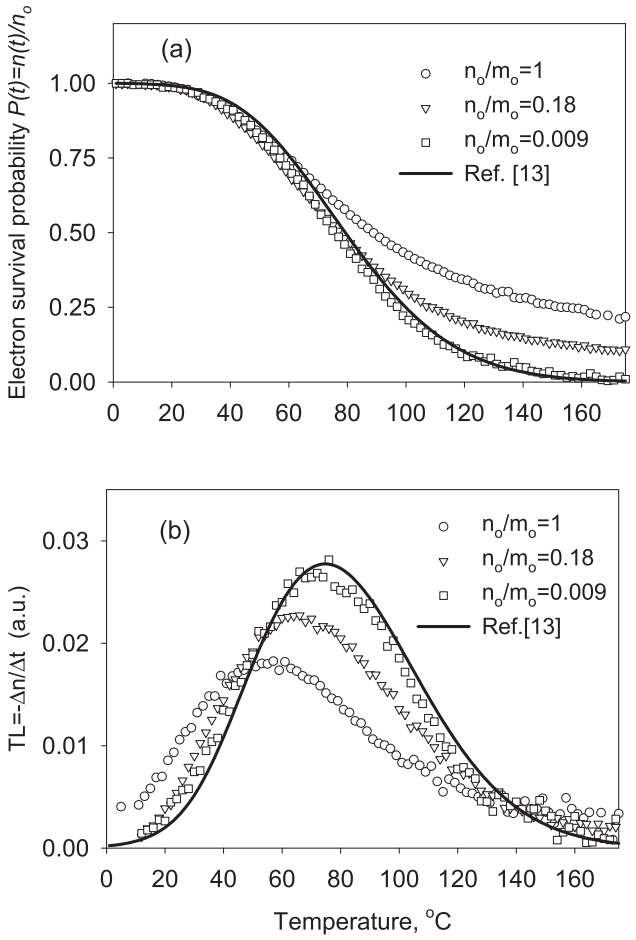

Fig. 3. Monte Carlo simulation for the same spherical distribution as in Fig. 2, by varying the relative initial concentrations of electrons and positive ions in the system. The initial number of positive ions inside the sphere is kept constant at $m_o = 1100$, while the initial number of electrons is varied. The solid lines correspond to the analytical Eqt (10), which is valid for very low values of the ratio n_o/m_o.

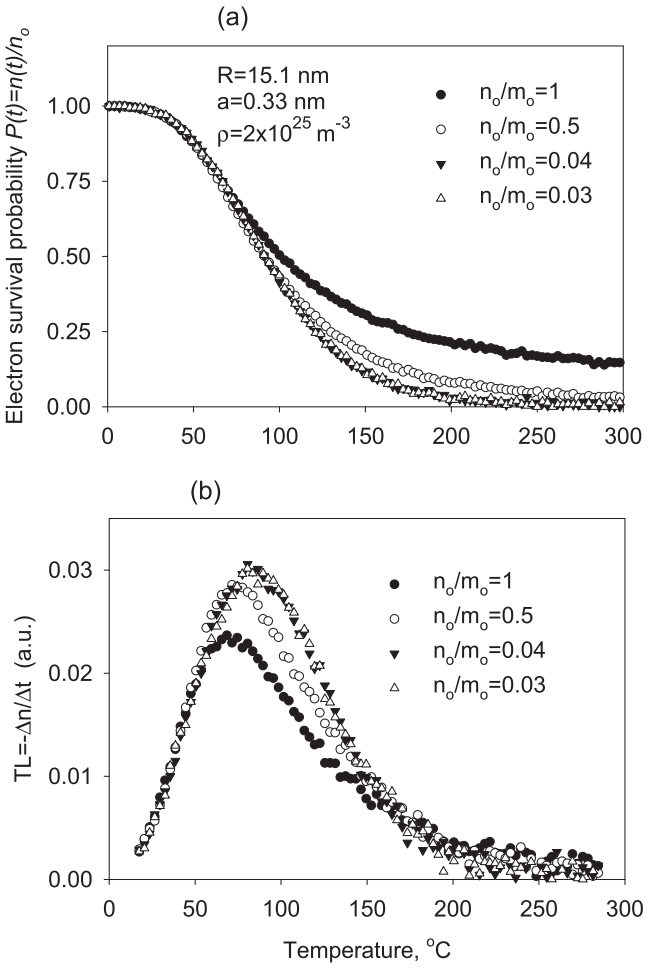

Fig. 4. A Monte Carlo simulation similar to Fig. 3, but for a different set of parameters in the model which are given in the text. The behavior of the TL glow curves is now different from the behavior iin Fig. 3; at low temperature region all TL glow curves are identical, while they differ in the high temperature region.

concentrations of electrons and positive ions in the system. The initial number of positive ions inside the sphere is kept constant at $m_o = 1100$ as in Fig. 2, while the initial number of electrons n_o is varied. The rest of the parameters in the model are kept constant. It is noted that there are no analytical expressions available in the literature for the TL glow curves shown in Fig. 3, except for the case $n_o/m_o \ll 1$. Monte Carlo is then the only available method of obtaining these results.

The simulated results in Fig. 3a show that as the ratio of initial concentrations n_o/m_o decreases, the tunneling process slows down. As a consequence, the corresponding TL glow curves in Fig. 3b become narrower and they shift towards higher temperatures. The solid lines in Fig.3ab correspond to the analytical Eqt (10), which is valid for very low values of the ratio n_o/m_o and for large crystals.

Fig. 4 shows a Monte Carlo simulation similar to Fig. 3, but for a different set of parameters in the model which correspond to a smaller crystal of radius $R = 15.1$ nm, tunneling length $a = 0.33$ nm, constant density of positive ions $\rho = 2x10^{25}$ m^{-3}, activation energy $E = 0.8$ eV, tunneling frequency $s = 3x10^{12}$ s^{-1}, a fixed value of $m_o = 70$ and a variable number of electrons n_o. The behavior of the TL glow curves in Fig. 4 is now different; at low temperature region all TL glow curves are identical, while their behavior is different at high temperature region.

The results in Figs. 3 and 4 are consistent with the Monte Carlo ground state simulations in Pagonis et al. [24], who showed that tunneling behavior in these random distributions of ions and electrons depends on a complex manner on the interplay of three lengths characterizing the system: the radius R, the tunneling length a, and on the average initial distance between electrons and ions (which is directly related to the concentration of charges).

3.3. *Monte Carlo simulations of TL in small nanocrystals with equal concentrations of electrons and positive ions*

Fig. 5 shows Monte Carlo simulations for a TL experiment in crystals with *equal* number of electrons and positive ions at all times. No analytical expressions for TL are available for such cases, and one must resort to a Monte Carlo simulation.

The initial density of electrons and positive ions in Fig. 5 is kept fixed at $\rho = 2x10^{25}\ m^{-3}$, while the initial number of charges is varied in the range $N = 3$–100, resulting in a variable radius R in the range $R = 5.3$-17.1 nm. The tunneling length $a = 0.33$ nm, density of positive ions $\rho = 2x10^{25}\ m^{-3}$, activation energy $E = 0.8$ eV, tunneling frequency $s = 3x10^{12}\ s^{-1}$. The arrows in Fig. 5 are in the direction of increasing radius R, and the solid lines are a guide to the eye.

The simulation in Fig. 5a shows that at low temperatures the tunneling process for small crystals is slower than in large crystals, with the arrows in Fig. 5a indicating the direction of increasing radius R. However, at higher temperatures the order of the curves is reversed, and the tunneling process for small crystals is now *faster* than in large crystals. This change of behavior leads to the simulated TL curves in Fig. 5b, in which the TL glow curves for smaller crystals are shifted towards higher

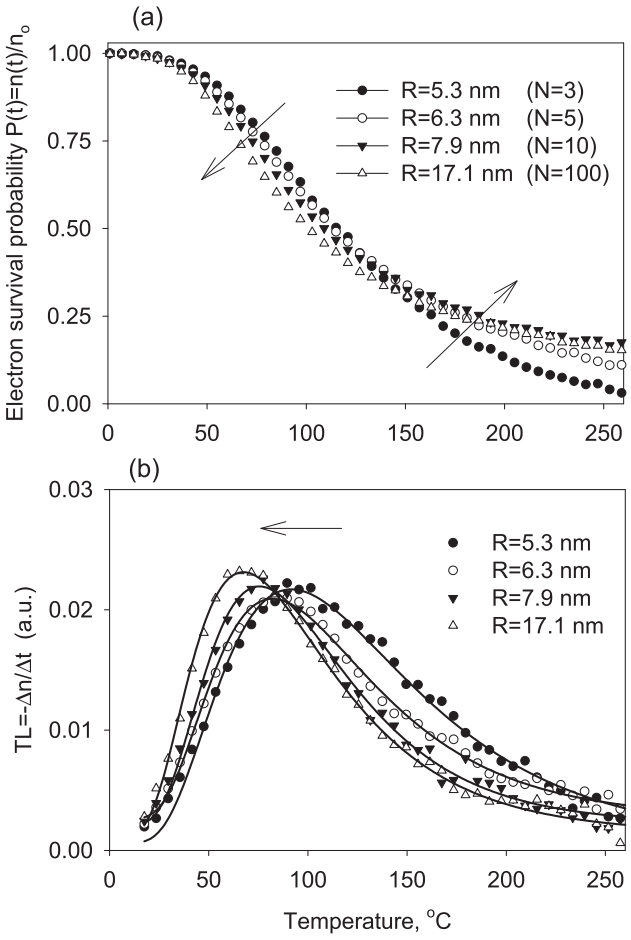

Fig. 5. Simulations for a TL experiment in crystals with *equal* number of electrons and positive ions at all times. (a) At low temperatures the tunneling process for small crystals is *slower* than in large crystals, with the arrows indicating the direction of increasing radius *R*. At higher temperatures the order of the curves is reversed. (b) The corresponding simulated TL curves. The solid lines are a guide to the eye.

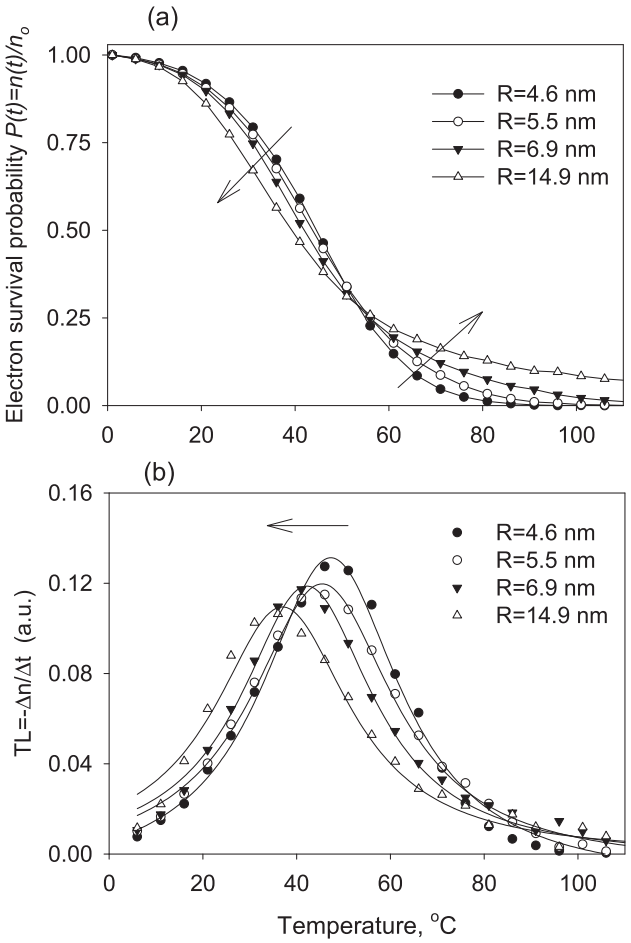

Fig. 6. The same type of simulations as Fig. 5, for a smaller tunneling length $a = 1\ nm$ while keeping all the other parameters fixed. The TL height as a function of the radius *R* in Fig. 6 shows the opposite behavior than the corresponding curves in Fig. 5. The solid lines are a guide to the eye.

temperatures, the TL height gets smaller, and the width becomes slightly larger. The area under the TL glow curves stays the same, since the survival probabilities *P(t)* in Fig. 5a are normalized at time $t = 0$, and the TL glow curves in Fig. 5b represent the derivatives of the normalized curves in Fig. 5a.

Fig. 6 shows the same type of simulations as Fig. 5, for a larger tunneling length $a = 1$ nm while keeping all the other parameters fixed. The simulations in Fig. 6 shows a different behavior for the TL height than the corresponding curves in Fig. 5. The TL height for smaller crystals gets larger, while the overall TL glow curve shifts towards higher temperatures, in a behavior similar to Fig. 5. The behavior of the curves in Figs. 5a and 6a is similar to the recently simulated ground state tunneling phenomena by Pagonis et al. ([24], their Fig. 9).

3.4. Examination of the nearest neighbor (NN) approximation

All simulations shown in Figs. 2–6 are based on the assumption of nearest neighbor interaction (NN). Pagonis et al. [24] presented ground state Monte Carlo simulations for crystals in which this assumption is lifted, i.e. when electrons are allowed to interact with all neighbors (ALLN). For the low densities used in their study, Pagonis et al. [24] found no significant differences between NN and ALLN simulations.

Fig. 7a compares simulated TL glow curves for NN and ALLN interactions and for a rather high initial charge density $\rho = 10^{25}\ m^{-3}$, and for equal concentrations of electrons and positive ions (N = 100). The simulation method and adjustments to the computer code for ALLN interactions were discussed recently in Pagonis et al. [24]. One might expect that the NN assumption will be a good approximation in general, unless one is dealing with extremely high charge densities (REF. [27]).

Fig. 7b compares Monte Carlo calculations carried out by using the NN and ALLN interactions, at a much lower density $\rho = 10^{23}\ m^{-3}$. As might be expected by physical arguments, the differences between NN and ALLN curves are more prominent in Fig. 7a than in Fig. 7b, due to the larger initial charge density in Fig. 7a.

3.5. Simulations of LM-IRSL experiments

In this section we consider simulations of LM-IRSL experiments, which have been carried out for a variety of materials (Bulur [29], Bulur and Goksu [28]).

In the case of LM-IRSL excitation modes, the rate of optical excitation is varied linearly with time in the form $\lambda_{LM\text{-}IRSL}(t) = bt$, where b is a constant which depends on the experimental conditions and on the optical cross section of the infrared light excitation. Jain et al. [25] demonstrated that for this type of experiment, Eqt (2) must be replaced by the following Arrhenius type of expression (Jain et al. [25], their Eqts.3 and 6):

$$\lambda(r,t) = s\exp[-r/a]\lambda_{LM-IRSL}(t) = s\exp[-r/a]bt. \quad (11)$$

It is again noted that Eqt (11) is derived by assuming quasi-static equilibrium conditions (QE) in the excited state tunneling model of Fig. 1c [22,23,25]. By combining Eqts (1) and (11) we obtain:

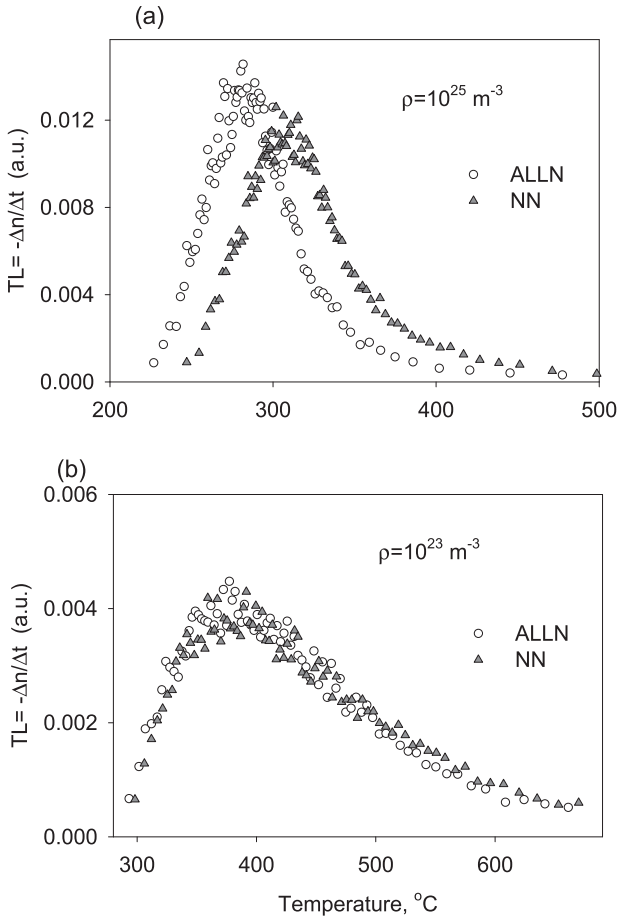

Fig. 7. Comparison of TL glow curves for NN and ALLN interactions, and for equal concentrations of electrons and positive ions. (a) Simulations for a high initial charge density $\rho = 10^{25}\, m^{-3}$. The simulation method and adjustments to the computer code for ALLN was discussed recently in Pagonis et al. [24]. (b) The same simulations as in (a), at a much lower density $\rho = 10^{23}\, m^{-3}$. The differences between NN and ALLN curves are more prominent in (a) than in (b).

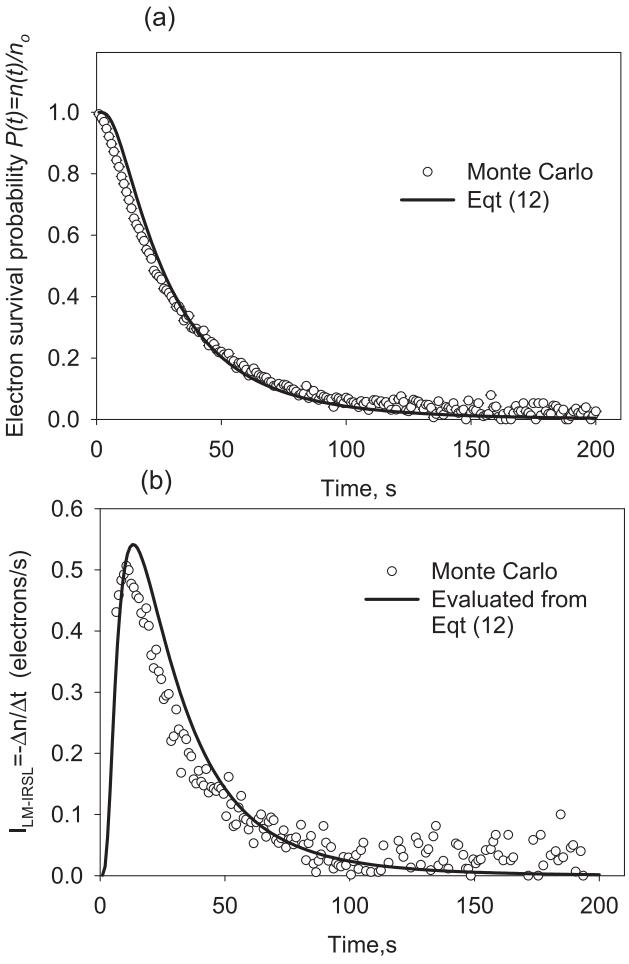

Fig. 8. Simulations of a typical LM-IRSL experiments, with the parameters in the model given in the text.

$$s\,\exp[-r/a]\int_0^{t_i} bt'dt' = -\ln(a_i). \tag{12}$$

In this case the integral in Eqt (12) can be evaluated analytically to obtain the time t_i, and Eqt (6) now becomes:

$$s\,\exp[-r_{MIN}/a]\frac{bt_i^2}{2} = -\ln(a_i). \tag{13}$$

Eqt (13) is the main equation used to evaluate the times t_i for recombination events during the LM-IRSL process. Its solution is obtained numerically in each step of the Monte Carlo simulation and for each remaining electron in the system, as was discussed previously for TL processes, with only the electron-ion pair corresponding to the shortest time being allowed to recombine.

Fig. 8 shows simulations of LM-IRSL experiments, by using the following parameters in the model: $R = 55.1\ nm,\ n_o = 20,\ m_o = 1100,\ a = 0.71\ nm,\ b = 6\ s^{-1},\ \rho = 6x10^{24}\, m^{-3}$.

The solid line in Fig.8ab represent the following analytical equation obtained by Kitis and Pagonis [14] for linearly modulated excitation modes:

$$P(t) = \exp\left[-\{4\pi\rho a^3/3\}\left[\ln\left\{1 + 1.8\frac{bt^2}{2T}\right\}\right]^3\right] \tag{14}$$

As in the case of TL, Eqt (14) is valid for *large* crystals, and it was derived by Kitis and Pagonis [14] from approximating the system of differential equations in the model by Jain et al. [13]. Good agreement can be seen between the Monte Carlo simulations and the analytical Eqt (14); the observed differences are likely due to the discrete nature of the Monte Carlo simulations.

4. Discussion and conclusions

The TL Monte Carlo simulations in this paper were tested by using the analytical equations developed by Kitis and Pagonis [14], which are valid for large crystals with nearest neighbor interactions, and for cases where the concentration of electrons is much smaller than the concentration of positive ions ($n_o \ll m_o$). There are no analytical equations available in the literature for the simulations shown in Figs. 4–7 of this paper.

Fig. 3 shows that changes of relative concentrations of electrons and positive ions lead to changes in the shape of the TL glow curves, and also in a shifting of the whole TL peak along the temperature scale. This behavior in Fig. 3 is different from that of Fig. 4, in which only the high temperature side of the TL peak changes, while the low temperature side remains unchanged. The two different behaviors seen in Figs. 3 and 4 are likely due to competition effects between the tunneling recombination process and the thermal excitation process at the different temperature ranges. Mathematically this competition process is expressed by the two terms *sexp(-r/a)* and *exp[-E/(k$_B$T)]* in Eqt (3) of this paper. The term for tunneling recombination *sexp(-r/a)* is temperature independent, while the term for thermal excitation rate *exp[-E/(k$_B$T)]* is strongly temperature dependent during the TL experiments.

This paper does not consider the effect of retrapping of charge carriers

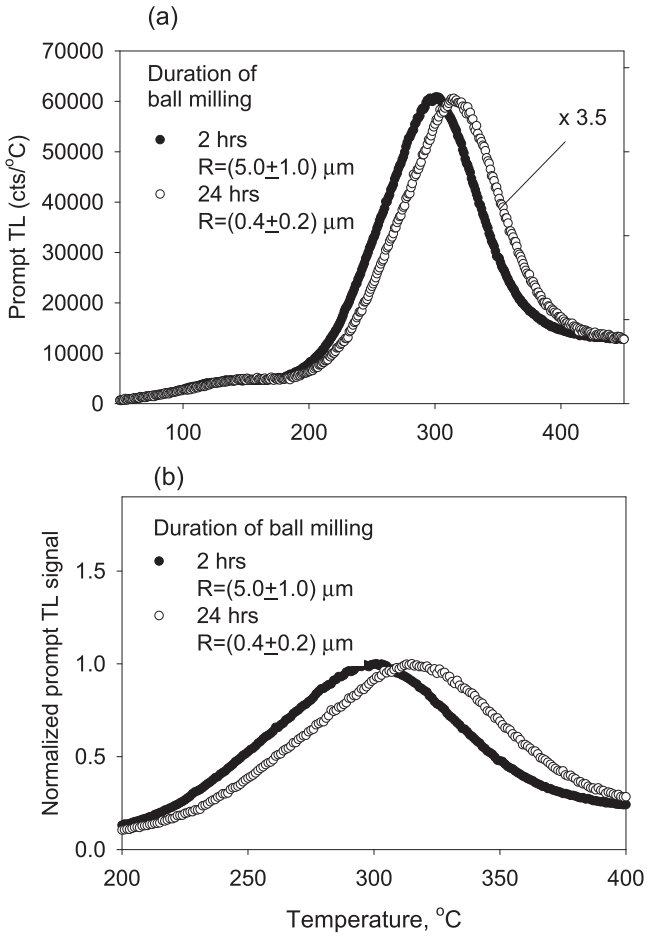

Fig. 9. Experimental TL glow curves for the same Durango apatite sample which has undergone ball milling for 2 h (dark circles, larger crystals) and 24 h (open circles, smaller crystals) [19]. (a) The complete TL glow curves (b) Detailed view of the normalized signals from (a), between 200 and 400 °C. The behavior of the TL glow curves is to be compared with the simulated behavior in Fig. 5.

in empty traps, which is assumed to be negligible here. However, it is necessary to include retrapping effects retrapping effects in future versions of the present model, since extensive experimental work on a variety of dosimetric materials has shown that the shape and position of TL peaks in the glow curve depend on the size of the nanocrystals. And also on the percent concentrations of various dopants. In addition, the TL glow curves for microcrystalline and nanocrystalline materials can be very different (see for example [1–4,30,31]).

It is interesting to compare the simulations in Fig. 5 with the recent experimental data of Polymeris et al. ([19], under review) on Durango apatite, a material which exhibits strong tunneling phenomena. In recent experiments these authors found that ball milling of Durango apatite powders for up to 48 h, resulted in significant changes in the TL and OSL luminescence signals in this material. Fig. 9 shows some of the experimental TL glow curves measured by Polymeris et al. ([19]) for the same Durango apatite sample which has undergone ball milling for 2 h (dark circles) and 24 h (open circles). The sample was irradiated with a small test dose after the end of the ball milling process, and its prompt TL signal was measured immediately after. Fig. 9a shows the complete normalized TL glow curves for the two ball milling times, while Fig. 9b shows details of the same data between 200 and 400 °C. The main peak in the TL glow curve for the smaller crystals with an average grain size R=(0.4 ± 0.2) μm, is shifted towards higher temperatures than the TL for larger crystals with average grain size R=(5.0 ± 1.0) μm. The *qualitative* behavior of the TL glow curves in Fig. 9 is very similar to the simulated behavior shown in Fig. 5, although the temperature and radius scales are very different. The grain sizes in Ref. [19] were obtained by analyzing scanning electron microscope images (SEM) of the ball milled sample. It is also noted that additional prompt TL glow curves (not shown in Fig. 9) for ball milling times of 4,8,12 h were also measured, and were found to be identical to the TL glow curves for a ball milling time of 2 h. This comparison of experimental data with the Monte Carlo model in this paper is very encouraging, and additional work is needed to produce quantitative agreement between experiment and theory.

The results in this paper are consistent with our recent Monte Carlo studies using the tunneling model in Fig. 1b. Specifically the crystal size effect shown in Figs. 5a and 6a of this paper, is very similar to Fig. 9 in the Monte Carlo ground state simulations in Pagonis et al. [24]. However, Fig. 8 in Pagonis et al. [24] showed a very different behavior of the electron survival probability as a function of time, in which larger crystals showed faster tunneling rate. This type of simulated behavior in Fig. 8 of Pagonis et al. [24] was *not* observed in the simulations of this paper. Nevertheless, it is possible that this different type of behavior would be observed by using a different set of parameters in the model.

Overall the Monte Carlo simulations in this paper and in Pagonis et al. [24] show that the tunneling behavior in random distributions of ions and electrons depends on a complex manner on the interplay of three lengths characterizing the system: the radius of the crystal R, the effective tunneling length $L_{eff} = 5a$, and the average distance $d> = 0.542\rho^{-1/3}$ in the distribution of nearest neighbors [24]. For a detailed discussion of the importance of these characteristic lengths in the context of tunneling phenomena in chemical physics, the reader is referred to the book by Gol'danskii et al. [27].

It is concluded that the simulations and analytical considerations in this paper can help researchers understand the origin and physical characteristics of the optically and thermally stimulated luminescence signals reported in a variety of nanodosimetric materials.

Acknowledgement

We thank Dr George Polymeris for providing us with the experimental data shown in Fig. 9.

References

[1] K.V. Eeckhout, P.F. Smet, D. Poelman, Materials 3 (2010) 2536–2566.
[2] V. Pagonis, R. Chen, C. Kulp, G. Kitis, Radiat. Meas. 106 (2017) 3–12.
[3] N. Salah, Nanocrystalline materials for the dosimetry of heavy charged particles: a review, Radiat. Phys. Chem. 80 (2011) 1–10.
[4] H.T. Sun, Y. Sakka, Sci. Technol. Adv. Mater. 15 (2014), 014205, https://doi.org/10.1088/1468–6996/15/1/014205.[3].Salah.
[5] I. Eliyahu, Y.S. Horowitz, L. Oster, S. Druzhyna, I. Mardor, Radiat. Meas. 71 (2014) 226–231.
[6] A. Mandowski, J. Swiatek, J. Philos. Mag. B65 (1992) 729–732.
[7] A. Mandowski, J. Swiatek, Radiat. Meas. 29 (1998) 415–419.
[8] A. Mandowski, Radiat. Meas. 33 (2001) 745–749.
[9] A. Mandowski, Radiat. Meas. 43 (2008) 199–202.
[10] A. Larsen, S. Greilich, M. Jain, A.S. Murray, Radiat. Meas. 44 (2009) 467.
[11] N.R.J. Poolton, R.H. Kars, J. Wallinga, A.J.J. Bos, J. Phys. Condens. Matter 21 (2009) 485505.
[12] V. Pagonis, M. Jain, K.J. Thomsen, A.S. Murray, J. Lumin. 153 (2014) 96–103.
[13] M. Jain, B. Guralnik, M.T. Andersen, J. Phys. Condens. Matter 24 (2012), 385402 (12pp).
[14] G. Kitis, V. Pagonis, J. Lumin. 137 (2013) 109–115.
[15] I.K. Sfampa, G.S. Polymeris, V. Pagonis, E. Theodosoglou, N.C. Tsirliganis, G. Kitis, Nucl. Instrum. Meth. Phys. Res. B 359 (2015) 89–98.
[16] G.S. Polymeris, N. Tsirliganis, Z. Loukou, G. Kitis, Phys. Status Solidi (a) 203 (2006) 578.
[17] V. Pagonis, C. Kulp, J. Lumin. 181 (2017) 114–120.
[18] I.K. Sfampa, G.S. Polymeris, N.C. Tsirliganis, V. Pagonis, G. Kitis, Nucl. Instrum. Meth. Phys. Res. B 320 (2014) 57–63.
[19] G.S. Polymeris, I.K. Sfampa, M. Niora, E.C. Stefanaki, L. Malletzidou, V. Giannoulatou, V. Pagonis, G. Kitis, Radiat. Meas. (2017), https://doi.org/10.1016/j.jlumin.2017.11.034 (in press).
[20] M. Tachiya, A. Mozumder, Chem. Phys. Lett. 28 (1974) 87.
[21] V. Pagonis, C. Kulp, C. Chaney, M. Tachiya, J. Phys. Condens. Matter 29 (2017) 365701.
[22] P. Thioulouse, E.A. Giess, I.F. Chang, J. Appl. Phys. 53 (1982) 9015.
[23] I.F. Chang, P. Thioulouse, J. Appl. Phys. 53 (1982) 5873.

[24] V. Pagonis, S. Bernier, F. Vieira, S. Steele, Nucl. Instrum. Meth. Phys. Res. B 412 (2017) 198–206.
[25] M. Jain, R. Sohbati, B. Guralnik, A.S. Murray, M. Kook, T. Lapp, A.K. Prasad, K.J. Thomsen, J.P. Buylaert, Radiat. Meas. 81 (2015) 242–250.
[26] R. Chen, V. Pagonis, Thermally and Optically Stimulated Luminescence: a Simulation Approach, Wiley and Sons, Chichester, 2011.
[27] V.I. Gol'danskii, L.I. Trakhtenberg, V.N. Fleurov, Tunneling Phenomena in Chemical Physics, Gordon and Breach Science publishers, New York, 1988.
[28] E. Bulur, H.Y. Goksu, Infrared (IR) stimulated luminescence from feldspars with linearly increasing excitation light intensity, Radiat. Meas. 30 (1999) 505–512.
[29] E. Bulur, Radiat. Meas. 26 (1996) 701–709.
[30] L.R. Singh, S.D. Singh, J. Nanomater. (2012), 239182, https://doi.org/10.1155/2012/239182.
[31] W. Chen, Z. Wang, Z. Lin, L. Lin, J. Appl. Phys. 82 (no. 6) (1997) 3111–3115.